

A regularization approach for the analysis of RHESSI X-ray spectra

A. M. Massone¹, M. Piana², A. Conway^{3,5}, and B. Eves⁴

¹ INFN, Unità di Ricerca di Genova, via Dodecaneso 33, I-16146 Genova, Italy
e-mail: massone@ge.infn.it

² INFN and Dipartimento di Matematica, Università di Genova, via Dodecaneso 35, I-16146 Genova, Italy
e-mail: piana@dim.unige.it

³ Department of Physics, Open University, Milton Keynes MK7 6AA, UK
e-mail: a.j.conway@open.ac.uk

⁴ Department of Physics, Open University, Milton Keynes MK7 6AA, UK
e-mail: b.a.c.eves@open.ac.uk

⁵ Department of Physics and Astronomy, The University, Glasgow G12 8QQ, UK
e-mail: andrew@astro.gla.ac.uk

the date of receipt and acceptance should be inserted later

Abstract. The Ramaty High Energy Solar Spectroscopic Imager (RHESSI) mission provides high resolution X-ray spectra emitted by collisional bremsstrahlung of electrons with the ions of the plasma. One of the aims of the mission is to infer information about the acceleration and transport mechanisms of electrons and ions in solar flares. Within the framework of an optically thin model and under the assumption of isotropic conditions in the solar plasma, the emitted photon spectrum is related to the electron flux density spectrum by an integral equation of the first kind. This problem is characterized by a notable numerical instability as a consequence of the experimental errors in the measured photon data. We address the solution of this problem by using the Tikhonov regularization algorithm. The method is applied to the case of three photon spectra registered by RHESSI detectors in the first months of the observational activity of the satellite. Furthermore a comparison of the reconstructions provided by the algorithm is performed in the case of the Kramers, Bethe-Heitler and Bethe-Heitler with the Elwert correction models for the bremsstrahlung cross-section.

Key words. solar flares – X-rays – inverse problems – regularization

1. Introduction

RHESSI (Ramaty High Energy Solar Spectroscopy Imager) is an imaging spectroscopy providing two-dimensional X-ray images of the solar atmosphere and one-dimensional hard X-ray spectra and γ -rays lines emitted during solar flares. In particular, the RHESSI mission was launched by NASA on February 5 2002 with the aim of providing crucial insights in the modeling of solar flares, by combining 2D imaging with the spectral information given by high-resolution Ge detectors.

Solar flares are transient phenomena characterized by the sudden release of huge amounts of energy. The typical manifestations of a solar flare are:

- acceleration of particles in the solar plasma;
- heating of the solar chromosphere;
- significant electromagnetic emission, particularly in the X-ray range.

One of the most challenging problems in solar physics is the determination of the dynamical origin of flares. In particular, in all the most reliable theoretical models (stochastic processes such as Fermi acceleration, DC electric field acceleration and Maxwellian bulk heating) the shape of the energy spectrum of the accelerated particles is a key to investigate the type of acceleration mechanism involved. In fact the RHESSI scientific objectives are:

- to determine the location and mechanism of particle acceleration in flares with particular emphasis on hard X-rays in the case of electron acceleration and γ -ray lines in the case of proton and ion acceleration;

Send offprint requests to: M. Piana

- to study the relation between particle acceleration and plasma heating;
- to study the particle and energy transport phenomena during flares.

Since the seminal papers by Brown (1971) and Lin (1974), it is well established that the dominant X-ray emission mechanism during solar flares is collisional bremsstrahlung of electrons with the ions of the low density atmospheric plasma. Our analysis is focused on the case of optically thin bremsstrahlung radiation (Brown & Emslie 1988), so that absorption can be neglected; furthermore we assume that the electron velocity distribution is characterized by isotropic conditions and, finally, that the plasma is hydrogen dominated, so that the ions are almost all protons. Under these conditions the bremsstrahlung source can be described in terms of the proton density $n(\mathbf{r})$ (cm^{-3}) and the differential flux $F(E, \mathbf{r})$ (electrons $cm^{-2} s^{-1} keV^{-1}$) at the non-relativistic energy E , both at position \mathbf{r} within the source volume V . Then the rate of emission of photons per unit ϵ is (Craig & Brown 1986)

$$g(\epsilon) = \bar{n}V \int_{\epsilon}^{\infty} f(E)Q(\epsilon, E)dE \quad , \quad (1)$$

where

$$\bar{n} = \frac{1}{V} \int_V n(\mathbf{r})dV \quad , \quad (2)$$

$$f(E) = \frac{1}{\bar{n}V} \int_V n(\mathbf{r})F(E, \mathbf{r})dV \quad (3)$$

and $Q(\epsilon, E)$ is the bremsstrahlung cross-section differential in photon energy. A rather complete survey of possible analytical forms for $Q(\epsilon, E)$ is given in (Koch & Motz 1959). Here we will consider three different cross-sections: the Kramers formula

$$Q(\epsilon, E) = \begin{cases} 0 & E \leq \epsilon \\ \frac{Q_0}{\epsilon E} & E > \epsilon \end{cases} \quad (4)$$

and the Bethe-Heitler formula

$$Q(\epsilon, E) = \begin{cases} 0 & E \leq \epsilon \\ \frac{Q_0}{\epsilon E} \log \frac{1+\sqrt{1-\epsilon/E}}{1-\sqrt{1-\epsilon/E}} & E > \epsilon \end{cases} \quad (5)$$

with

$$Q_0 = \frac{8}{3} \frac{r_0^2}{137} mc^2 \quad ; \quad (6)$$

and the Bethe-Heitler formula with the Elwert correction (Johns & Lin 1992a; Johns & Lin 1992b)

$$Q(\epsilon, E) = \begin{cases} 0 & E \leq \epsilon \\ Q_1 q_1(\epsilon, E) q_2(\epsilon, E) q_3(\epsilon, E) q_4(\epsilon, E) q_5(\epsilon, E) & E > \epsilon \end{cases} \quad , \quad (7)$$

with

$$Q_1 = \frac{Z^2 r_0^2}{137} \frac{16}{3} \quad ; \quad (8)$$

$$q_1(\epsilon, E) = \frac{m^2 c^4}{\epsilon E(E + 2mc^2)} \quad ; \quad (9)$$

$$q_2(\epsilon, E) = \log \left[\frac{1 + \left(\frac{(E-\epsilon)(E-\epsilon+2mc^2)}{E(E+2mc^2)} \right)^{1/2}}{1 - \left(\frac{(E-\epsilon)(E-\epsilon+2mc^2)}{E(E+2mc^2)} \right)^{1/2}} \right] \quad ; \quad (10)$$

$$q_3(\epsilon, E) = [E(E + 2mc^2)]^{1/2} [E - \epsilon + mc^2] \quad ; \quad (11)$$

$$q_4(\epsilon, E) = \left\{ 1 - \exp \left[-\frac{2\pi(E + mc^2)}{137[E(E + 2mc^2)]^{1/2}} \right] \right\} \quad ; \quad (12)$$

$$q_5(\epsilon, E) = \left\{ [(E - \epsilon)(E - \epsilon + 2mc^2)]^{1/2} [E + mc^2] \left\{ 1 - \exp \left[-\frac{2\pi(E - \epsilon + mc^2)}{137[(E - \epsilon)(E - \epsilon + 2mc^2)]^{1/2}} \right] \right\} \right\}^{-1} \quad . \quad (13)$$

In equations (6)-(13), Z represents the atomic number of the ion with which the electron collides, r_0 is the classical electron radius, m is the rest mass of the electron and c is the speed of light.

In real applications only a finite set of integrals of the photon spectrum over small photon energy intervals is available. However, if these intervals are small compared with the resolution implied by the smoothing kernel (i.e., the cross-section), the integration effect provided by the detectors can be neglected and the equation describing the emission process is, rather realistically,

$$g(\epsilon_n) = \int_{\epsilon_n}^{\infty} Q(\epsilon_n, E)f(E)dE \quad n = 1, \dots, N \quad . \quad (14)$$

The problem of determining the unknown electron spectrum $f(E)$ from the knowledge of the photon data set $\{g_n\}_{n=1}^{\infty}$ is a typical example of linear ill-posed inverse problem with discrete data (Bertero *et al.* 1985; Bertero *et al.* 1988). Without focusing on the technical definition (Hadamard 1923), in this context ill-posedness essentially means two facts: first, the solution of the problem is not unique since there are infinitely many functions fitting the photon data in equation (14); second, when the data are affected by experimental noise, a *naive* inverse approach to the solution of the problem induces heavy numerical instabilities which make the restored flux density spectrum completely unreliable from a physical point of view. In order to obtain the maximum benefit from RHESSI data we think that it is essential to deal with this inverse problem by allowing for its ill-posed nature. In particular we believe that the only way to systematically handle both the ambiguity involved by the non-uniqueness of the solution and the numerical instability induced by the presence of noise on the data is to apply numerical techniques based on the regularization theory for linear ill-posed inverse problems. A description of the regularization theory approach in this context can be found in (Piana 1994). The basic requirement of such an approach is to solve the minimum problem

$$\|Af - \mathbf{g}\|^2 + \lambda\|f\|^2 = \text{minimum} \quad , \quad (15)$$

where (Af) is a vector with components

$$(Af)_n = \int_{\epsilon_n}^{\infty} Q(\epsilon_n, E)f(E)dE \quad , \quad (16)$$

\mathbf{g} is a vector with components $g_n = g(\epsilon_n)$ and the norms are taken in the appropriate spaces. On the left hand side of equation (15), the first term measures the fitting accuracy while the second term introduces a constraint on the size of the solution, suppressing large departures from a smooth electron spectrum and therefore is concerned with stability. The regularization parameter $\lambda > 0$ tunes the trade-off between approximation and stability. In Piana (1994) the Tikhonov (1963) regularization method has been applied for the solution of equation (14) only with the Bethe-Heitler cross-section in the case of the X-ray spectrum registered during the June 27 1980 flare by Ge detectors placed on a balloon. In the present paper we will follow an analogous approach in the case of the high-resolution RHESSI spectra, this time by considering the Kramers cross-section and the Elwert correction, too. More precisely, in Section 2 three different RHESSI spectra, registered in the first months of the satellite's flight, will be inverted by using the Tikhonov algorithm. Then, in Section 3, we will discuss the main advantages of using a regularized inversion technique. Finally Section 4 will contain a discussion of the results. In Appendix A an overview of the Tikhonov method within the framework of the linear inverse problem theory will be given.

2. RHESSI spectra: application of Tikhonov method

Tikhonov regularization theory is a two-step inversion technique providing an optimal trade-off between stability and best-fitting. In the first step, many approximate reconstructions are obtained by solving problem (15) for different values of the regularization parameter λ . The second step consists in selecting one particular approximate reconstruction by means of an optimal choice of the parameter in the quadratic functional. The optimality criterion at the basis of this choice will be to tune this real positive number λ in order that the numerical oscillations are reduced but the compatibility with the observed data is preserved. A concise overview of the formalism of Tikhonov regularization theory is in Appendix A. The most notable advantages of this technique are that, first of all, very few *a priori* assumptions on the solution are necessary in the inversion procedure (namely, only that the electron flux density spectrum is as smooth as possible) and, moreover, that if conveniently implemented, the algorithm is efficient: our IDL code produces reconstructions of the electron spectrum from 90 point photon spectra in a few seconds.

We consider now the three photon spectra registered by RHESSI detectors on February 20 at 11:06, March 17 at 19:30 and August 6 at 12:56. The plot of these three data vectors is in Fig. 1. These data are characterized by RHESSI's highest spectral resolution of 1 keV bins in the 10 – 100 keV range (to obtain such a resolution, data from detectors 2 and 7 have been omitted since their resolution is poorer than that of RHESSI's other seven detectors). Furthermore we chose time bins equal to RHESSI's rotation period in order that there would be no modulation from the imaging grids. The standard software has been used to perform some pre-processing steps: detector energy response, detector lifetime, attenuator transmission and imaging grid transmission. The background has been subtracted by using the SPEX package to interpolate between two background intervals, one before and one after the flare. No thermal component has been subtracted, since in equations (1)-(3) $f(E)$ includes both the thermal and non-thermal contributions (Piana *et al.* 2003). Finally a pulse pile-up correction has been applied to the 17 March

Table 1. Optimal values of the regularization parameter for the three events under examination in the case of three different bremsstrahlung cross-sections. The choice criterion is the Morozov’s discrepancy principle.

	Kramers	Bethe-Heitler	Bethe-Heitler-Elwert
Feb 20	$\lambda = 2.8 \times 10^{-6}$	$\lambda = 1.2 \times 10^{-6}$	$\lambda = 3.4 \times 10^{-12}$
Mar 17	$\lambda = 1.3 \times 10^{-6}$	$\lambda = 4.3 \times 10^{-7}$	$\lambda = 1.7 \times 10^{-12}$
Aug 6	$\lambda = 5.5 \times 10^{-6}$	$\lambda = 2.1 \times 10^{-6}$	$\lambda = 7.8 \times 10^{-12}$

2002 event, which is the largest flare in terms of GOES class (the software and data used were the most up-to-date available on 23rd January 2003). We have applied the Tikhonov regularization method to these three data sets in the case of Kramers, Bethe-Heitler and Bethe-Heitler with the Elwert correction cross-sections. Figure 2 (a) contains the reconstruction of $\bar{n}Vf(E)$ for the February 20 flare and the three models. In Fig. 2(b) and Fig. 2(c) the same quantity is reconstructed for the March 17 and August 6 events respectively. In the restoration procedure the regularization parameter has been fixed by means of the discrepancy principle (Tikhonov et al. 1995; see Appendix A). The optimal values for the three events and the three cross-sections are given in Table 1. Clearly, the selected values for the Bethe-Heitler-Elwert model are systematically smaller than the ones for the other two cross-sections. This result indicates that that when this cross-section is adopted, the problem is numerically more stable than in the other two cases, since, from equation (15), smaller values of the regularization parameter correspond to a smaller weight given to the stability term at the left hand side of the equation. As a confirmation of this fact, we have that the condition number associated to the linear equation (14) (see Appendix A) is smaller when $Q(\epsilon, E)$ is the Bethe-Heitler-Elwert cross-section ($\sim 10^2$) than when $Q(\epsilon, E)$ are the Kramers ($\sim 10^3$) or the Bethe-Heitler ($\sim 10^5$) cross-sections.

Figure 3 contains the electron flux density spectrum corresponding to the February 20 event for the three cross-sections. The vertical bars at each point have been obtained by computing the confidence strip corresponding to the photon spectrum, i.e. from repeated inversions of different random realizations of the photon spectrum for a fixed value of the regularization parameter. The width of the horizontal bars in the case of Kramers and Bethe-Heitler cross-sections (Fig. 3(a) and Fig. 3(b)) have been obtained as described in Appendix A. If the Elwert correction is adopted (Fig. 3(c)), the resolution bar is given by the discretization interval in the electron energy range. Figures 4 and 5 contain the electron flux density spectra corresponding to the March 17 and August 6 events.

3. Direct and inverse approaches

In solar physics literature the solution of equation (14) can be addressed without allowing for the ill-posedness of the inverse problem, for example according to the following two strategies:

1. a direct approach, whereby the photon spectrum is best-fitted by using *a priori* chosen parametrized forms for the electron spectrum
2. an inverse approach based on the discretization of analytical inversion formulas.

In the forward-fitting approach the photon spectrum is fitted by a simple function such as a power law to obtain a photon spectrum index γ and then either a thin- or a thick-target model is assumed to obtain an electron spectrum index δ . Such an approach gives the best power-law fit to the behaviour at high energies, but obviously cannot detect possible detailed features which may have a physical meaning or may be produced by systematic defects in the measurement procedure. Regularization techniques preserve such features and, in the meantime, reproduce the data vector with great accuracy. As an example, in Fig. 6(a) the data set corresponding to the February 20 flare (Fig. 1(a)) has been best-fitted by a power law with index $\delta \simeq 2.8$. In Fig. 6(b) the same spectrum is fitted with the regularized solution represented in Fig. 2(a) (solid line) obtained by using the Kramers cross-section. Clearly, the data fit provided by the Tikhonov regularized solution is more accurate than the one provided by the power law.

Simple inversion schemes for the solution of the solar bremsstrahlung problem can be obtained by analytically inverting equation (1) and then by discretizing the inversion formula. However, it is extremely difficult to obtain an analytical inversion formula in the case of a general cross-section. For example in Brown (1971), equation (1) is analytically solved for the Bethe-Heitler scattering, by showing that an appropriate change of variables leads to an Abel-type equation (Riesz & Nagy 1953); nevertheless, to our knowledge, there is no inversion formula for the same equation when also the Elwert correction is allowed for, as in equations (7)-(13). Furthermore, analytical inversion formulas typically involve expressions containing derivatives of the photon spectrum and therefore cannot be applied when the data are not known very accurately. In (Johns and Lin 1992a), an inversion method is proposed where an iterative procedure is obtained by exploiting the facts that bremsstrahlung spectra from optically thin sources always decrease with increasing photon energy, and electrons of a given energy can only produce photons of equal or lower energy. This method exploits the Volterra character of the original integral equation and is based on a standard row elimination technique, where a “local smoothing” procedure is applied *via* adjustable bin widths. This discretization-rebinning operation introduces a certain regularization effect whose intensity, however, is not chosen by means of some objective criterion,

as in the Tikhonov method. Therefore, if applied to real data affected by observational noise, this scheme may produce oscillating solutions, as shown in (Emslie *et al.* 2001).

4. Comments and open problems

In the present paper we have shown that the Tikhonov regularization algorithm is a potentially effective method for the reconstruction of electron flux density spectra from the photon spectra provided by the RHESSI Mission. In particular, this approach allows the suppression of the noise amplification due to the ill-posedness of the original inverse problem. Furthermore, many interesting features in the recovered $\bar{n}Vf$, which cannot be pointed out by means of forward-fitting approaches, are clearly preserved. For example, the March 17 spectrum presents a pronounced concavity for $E \geq 30$ keV while the February 20 spectrum presents a detailed feature just around 30 keV (more evident in the Bethe-Heitler and Bethe-Heitler-Elwert reconstructions). The origin and physical meaning of such features is a crucial problem currently under investigation (first steps in this direction are in (Piana *et al.* 2003)).

The problem of the dependence of the reconstructed electron spectrum from the cross-section is still open and certainly deserves a systematic study. For the three data sets considered in the present paper, there is a substantial independence from the model in the middle energy range. The upturn in solution f at highest E for some cross-sections is a numerical artefact of the truncation of the data and hence of our representation above 100 keV. This should be ignored until a dependable fix is added. At low energies, the Bethe-Heitler cross-section produces a downturn in $\bar{n}VF$ below 15 keV, which occurs also when the Haug (1997) model is adopted (Piana *et al.* 2003). This effect vanishes if the Elwert correction is introduced. The physical reliability of this feature is currently under investigation. From a more technical point of view, we would also like to investigate the sensitivity of the reconstructions to the values of the regularization parameters, by applying optimality criteria different from the discrepancy principle used in the present paper.

Acknowledgements. Part of this work was supported by a Royal Society grant. We want to thank Dr. E. Kontar for his help with the pile-up correction to the data.

Appendix A: Tikhonov method

In order to describe the main features of Tikhonov regularization algorithm we introduce some simple formalism typical of the theory of linear inverse problems. Let Y be the Euclidean data space equipped with the scalar product

$$(\mathbf{g}, \mathbf{h})_Y = \sum_{n=1}^N g_n h_n w_n \quad (\text{A.1})$$

where N is the dimension of the space, the w_n are appropriate weights and \mathbf{g} and \mathbf{h} are vectors in Y such that $\mathbf{g} = (g_1, \dots, g_n)$, $\mathbf{h} = (h_1, \dots, h_n)$. In our applications the photon spectrum is viewed as a vector \mathbf{g} in Y such that $g_n = g(\epsilon_n)$. Moreover, the weights are typically chosen according to the kind of sampling adopted in the measurement procedure. For example, in the case of the uniform data sampling with sampling distance equal to d

$$\epsilon_n = \epsilon_1 + d * (n - 1) \quad n = 1, \dots, N \quad , \quad (\text{A.2})$$

an efficient choice is given by

$$w_n = d \quad (\text{A.3})$$

while in the case of the geometrical data sampling with sampling ratio Δ

$$\epsilon_n = \epsilon_1 \Delta^{n-1} \quad n = 1, \dots, N \quad , \quad (\text{A.4})$$

the choice

$$w_n = (\log \Delta) \epsilon_n \quad (\text{A.5})$$

should be preferred. Let $A : X \rightarrow Y$ be defined by

$$(Af)_n = \int_0^\infty Q(\epsilon_n, E) f(E) dE \quad n = 1, \dots, N \quad . \quad (\text{A.6})$$

We assume $X = L^2(0, \infty)$ where $L^2(0, \infty)$ is the space of functions f satisfying

$$\int_0^\infty |f(x)|^2 dx < +\infty \quad (\text{A.7})$$

and equipped with the scalar product

$$(f_1, f_2)_X = \int_0^\infty f_1(x)f_2(x)dx \quad . \quad (\text{A.8})$$

The measured datum \mathbf{g}_η is a vector in Y which can be represented in the form

$$\mathbf{g}_\eta = Af^{(0)} + \mathbf{h} \quad (\text{A.9})$$

where $f^{(0)}$ is the ideal theoretical solution of the problem and \mathbf{h} such that $\|\mathbf{h}\|_Y = \eta$ describes the noise affecting the data as a consequence of the measurement procedures. We point out that the representation (A.9) is not necessarily additive since in principle \mathbf{h} may depend on $f^{(0)}$. In the case of a high signal-to-noise ratio the noise term in (A.9) can be neglected and the problem becomes the one to determine f from \mathbf{g}_η when f and \mathbf{g}_η are related by

$$\mathbf{g}_\eta = Af \quad . \quad (\text{A.10})$$

According to the Tikhonov algorithm a regularized solution of problem (A.10) must be looked for in the one-parameter family of solutions of the minimum problem

$$\|Af - \mathbf{g}_\eta\|_Y^2 + \lambda\|f\|_X^2 = \text{minimum} \quad (\text{A.11})$$

where λ is a real strictly positive number named the regularization parameter. In equation (A.11) the first term at the left hand side measures the fitting of the data while the second term measures the stability of the solution: it follows that for too large values of the regularization parameter the regularized solution will be characterized by an oversmoothed behaviour while for too small values of the regularization parameter it will be still affected by artifacts due to the numerical instability. The goal of an optimal choice of the regularization parameter is a crucial problem in regularization theory. To this aim in the present paper we will apply the Morozov's discrepancy principle (Tikhonov *et al.* 1995) according to which the optimal value of the regularization parameter is represented by the solution of the discrepancy equation

$$\|Af_\lambda - \mathbf{g}_\eta\|_Y = \eta \quad . \quad (\text{A.12})$$

In other terms, Morozov's criterion requires that the selected approximate solution fits the data within the order of magnitude of the noise.

The computation of both the regularized solution and Morozov's discrepancy principle is significantly facilitated by computing the Singular Value Decomposition (SVD) of the operator A . The singular system of A (Bertero *et al.* 1985) is defined as the set of triples $\{\sigma_k; \mathbf{v}_k, u_k\}_{k=1}^N$ such that the positive real singular values σ_k , the singular vectors \mathbf{v}_k in Y and the singular functions u_k in X satisfy the *shifted* eigenvalue problem

$$Au_k = \sigma_k \mathbf{v}_k \quad ; \quad A^* \mathbf{v}_k = \sigma_k u_k \quad k = 1, \dots, N \quad . \quad (\text{A.13})$$

It is easily proved that the solution of the minimum problem (A.11) can be expanded in the form

$$f_\lambda(E) = \sum_{k=1}^N \frac{\sigma_k}{\sigma_k^2 + \lambda} (\mathbf{g}_\eta, \mathbf{v}_k) u_k(E) \quad (\text{A.14})$$

and that the discrepancy equation (A.12) can be represented in the form

$$\sum_{k=1}^N \frac{\lambda^2}{(\sigma_k^2 + \lambda)^2} |(\mathbf{g}_\eta, \mathbf{v}_k)|^2 = \eta^2 \quad . \quad (\text{A.15})$$

In order to compute the singular system of A we have to distinguish between the case of the Kramers and Bethe-Heitler cross-sections and the case of the Bethe-Heitler-Elwert cross-section.

If the Kramers or Bethe-Heitler models are adopted, we introduce the real symmetric $N \times N$ Gram matrix G_{nm} defined by

$$G_{nm} = (Q(\epsilon_n, \cdot), Q(\epsilon_m, \cdot))_X \quad n, m = 1, \dots, N \quad . \quad (\text{A.16})$$

It is shown in (Bertero *et al.* 1985) that the factorization

$$AA^* = G^T W \quad (\text{A.17})$$

holds, where A^* is the adjoint operator of A defined by

$$(f, A^* \mathbf{g})_X = (Af, \mathbf{g})_Y \quad (\text{A.18})$$

and W is the weight matrix defined by

$$W_{nm} = w_n \delta_{nm} . \quad (\text{A.19})$$

From equations (A.16)-(A.19) and from the fact that (Bertero *et al.* 1985)

$$u_k(E) = \frac{1}{\sigma_k} \sum_{n=1}^N w_n (\mathbf{v}_k)_n Q(\epsilon_n, E) \quad (\text{A.20})$$

it follows that the problem of determining the singular system of A is reduced to the problem of diagonalizing the Gram matrix.

In the case of the Bethe-Heitler formula with the Elwert correction, the explicit form of the functions $Q(\epsilon_n, E)$ is too complicated to make the Gram matrix computation and diagonalization affordable. Therefore in this case we discretize equation (A.10) also in the electron energies and perform the SVD computation in a finite dimensional framework by means of a standard numerical routine. The availability of the singular spectrum of A allows to infer information about the instability of the inverse problem. In fact, the condition number, which provides a quantitative measure of such instability, is given by the ratio between the largest and the smallest singular value.

Note that equation (A.14) provides a simple way to estimate the energy resolution of the reconstructed electron spectrum. In fact, this is measured by the distance between two adjacent zeros in the last significant singular function, this being the last singular function providing a non-negligible contribution to the computation of the regularized solution by means of equation (A.14).

References

- Bertero, M., De Mol, C. & Pike, E. R. 1985, *Inverse Problems*, 1, 301
Bertero, M., De Mol, C. & Pike, E. R. 1988, *Inverse Problems*, 4, 573
Brown, J. C. 1971, *Solar Phys.*, 18, 489
Brown, J. C. & Emslie, A. G. 1988, *Ap. J.*, 331, 554
Craig, I. J. D. & Brown, J. C. 1986, *Inverse Problems in Astronomy* (Adam Hilger, Bristol)
Crannell, C. J., Frost, K. J., Mätzler, C., Ohki, I. & Saba, J. L. 1978, *Ap. J.*, 223, 620
Elcan, M. J. 1978, *Ap. J. (Letters)*, 226, L99
Emslie, A. G., Barrett, R. K. & Brown, J. C. 2001, *Ap. J.*, 557, 1
Hadamard, J. 1923, *Lectures on Cauchy's Problem in Linear Partial Differential Equation* (Yale University Press, New Haven)
Haug, E. 1997, *A&A*, 326, 417-418
Johns, C. M. & Lin, R. P. 1992, *Solar Phys.*, 137, 121
Johns, C. M. & Lin, R. P. 1992, *Solar Phys.*, 142, 219
Kane, S. R. & Anderson, K. A. 1970, *Ap. J.*, 162, 1002
Kane, S. R., Crannell, D., Datlowe, D., Feldman, U., Gabriel, A., Hudson, H. S., Kundu, M. R., Mätzler, C., Neidig, D., Petrosian, V. & Sheeley, N. R. 1980, in *Solar Flares*, ed. P. A. Sturrock (Associated University Press, Boulder)
Koch, H. W. & Motz, J. W. 1959, *Rev. Mod. Phys.*, 31, 920
Lin, R. P. 1974, *Space Sci. Rev.*, 16, 189
Lin, R. P. & Schwartz R. A. 1987, *Ap. J.*, 312, 462
Piana, M. 1994, *A&A*, 288, 949
Piana, M., Brown J. C. & Thompson A. M. 1995, *Solar Phys.*, 156, 315
Piana, M., Massone A. M., Kontar, E. C., Emslie, A. G., Brown, J. C. & Schwartz, R. A. 2003 (submitted to *Ap. J. (Letters)*)
Riesz, F. and Nagy, B. 1953, *Lecons d'analyse fonctionelle* (Akademiai Kiado, Budapest)
Tikhonov, A. N. 1963, *Sov. Math. Dokl.*, 4, 1035
Tikhonov, A. N., Goncharsky, A. V., Stepanov, V. V. and Yagola, A. G. 1995, *Numerical Methods for the Solution of Ill-posed Problems* (Kluwer, Dordrecht)

Figure captions

Figure 1. The RHESSI spectra: (a) data set registered on February 20 2002 at 11:06; (b) data set registered on March 17 2002 at 19:30; (c) data set registered on August 6 2002 at 12:56.

Figure 2. Tikhonov regularized solutions in the case of Kramers (solid), Bethe-Heitler (dashes) and Bethe-Heitler with Elwert correction (dots) cross-sections: (a) the February 20 event; (b) the March 17 event; (c) the August 6 event.

Figure 3. Tikhonov reconstructions in the case of the February 20 event. Also the error and resolution bars are shown: (a) the Kramers cross-section is adopted; (b) the Bethe-Heitler cross-section is adopted; (c) the Bethe-Heitler with Elwert correction is adopted.

Figure 4. Tikhonov reconstructions in the case of the March 17 event. Also the error and resolution bars are shown: (a) the Kramers cross-section is adopted; (b) the Bethe-Heitler cross-section is adopted; (c) the Bethe-Heitler with Elwert correction is adopted.

Figure 5. Tikhonov reconstructions in the case of the August 6 event. Also the error and resolution bars are shown: (a) the Kramers cross-section is adopted; (b) the Bethe-Heitler cross-section is adopted; (c) the Bethe-Heitler with Elwert correction is adopted.

Figure 6. Data fit of the February 20 event: (a) a power law is used in the forward-fitting approach; (b) the fit is obtained by inserting the Tikhonov regularized solution in equation (14) when the Kramers cross-section is adopted.

photon spectrum $g(\epsilon)$ ($\text{cm}^{-2} \text{s}^{-1} \text{keV}^{-1}$)

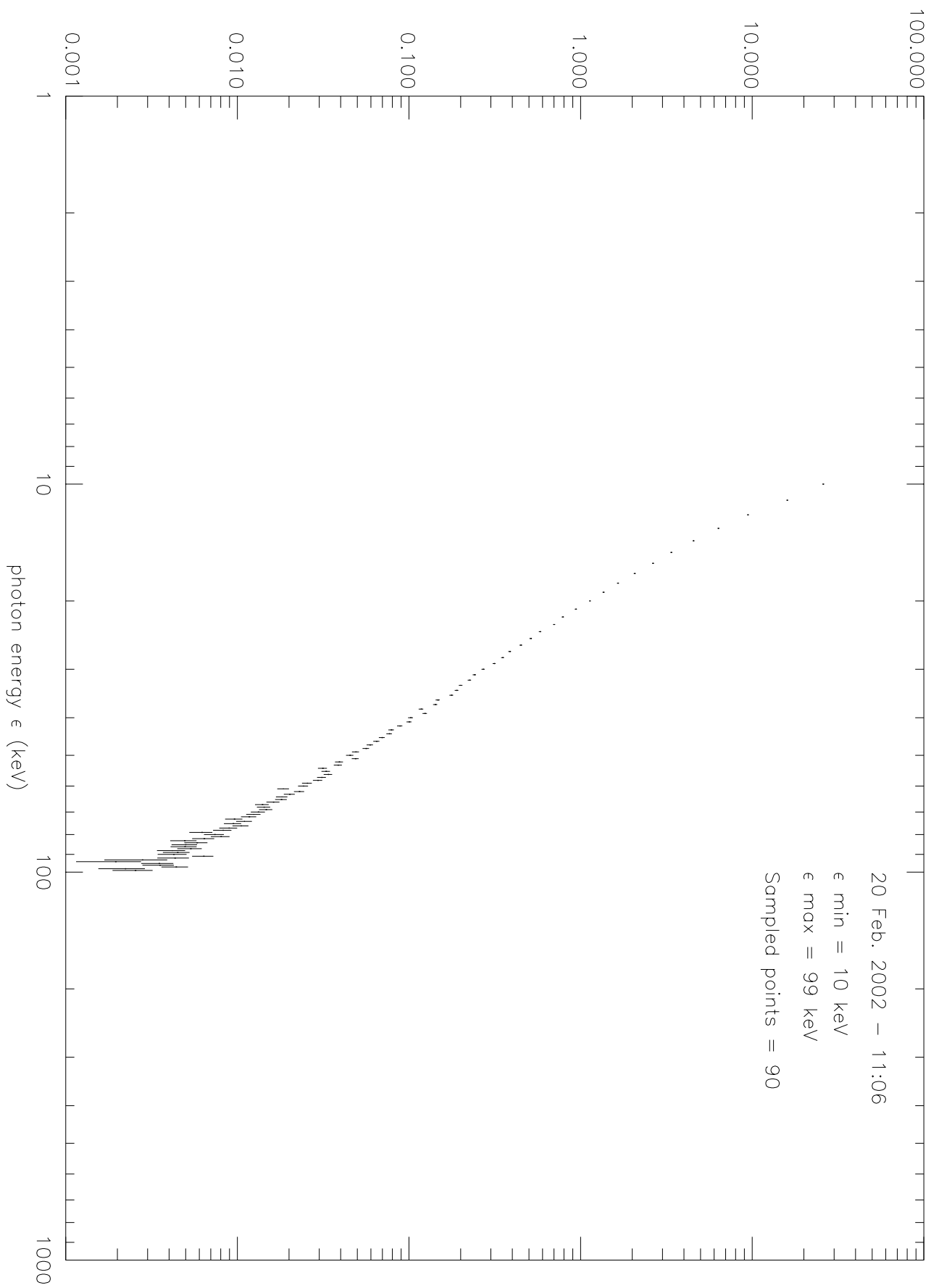


Fig. 1(a)

photon spectrum $g(\epsilon)$ ($\text{cm}^{-2} \text{s}^{-1} \text{keV}^{-1}$)

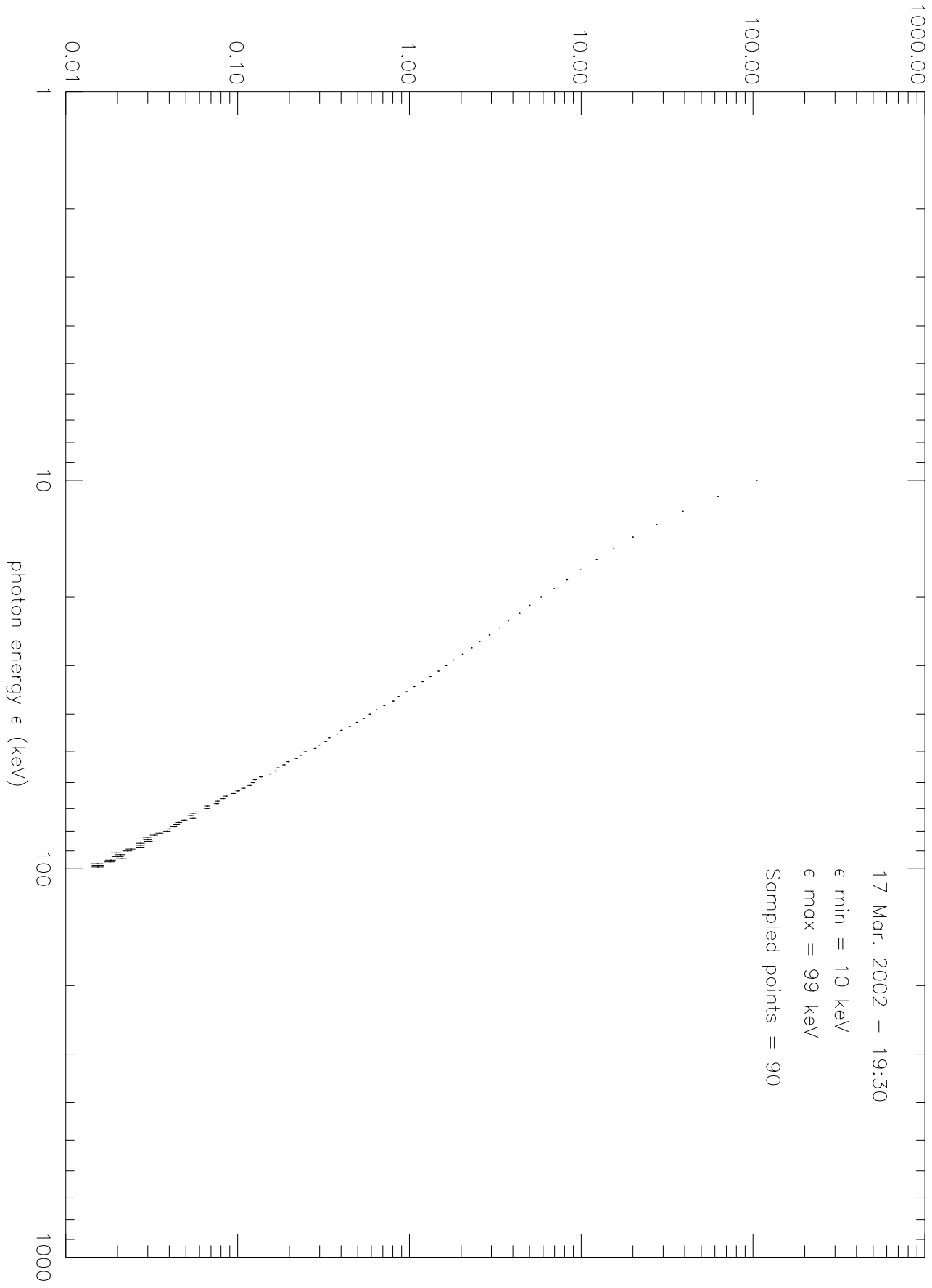


Fig. 1(b)

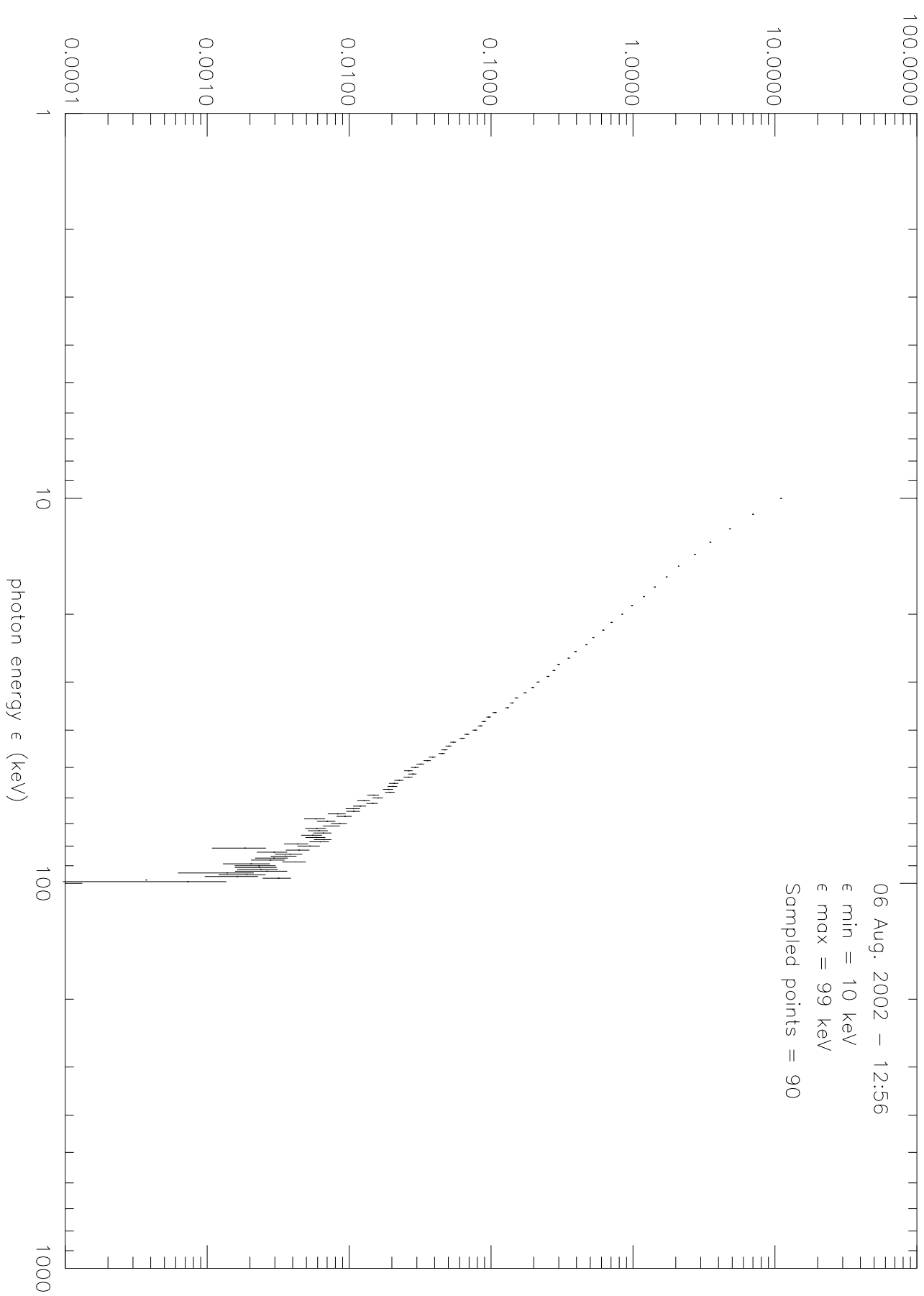


Fig. 1(c)

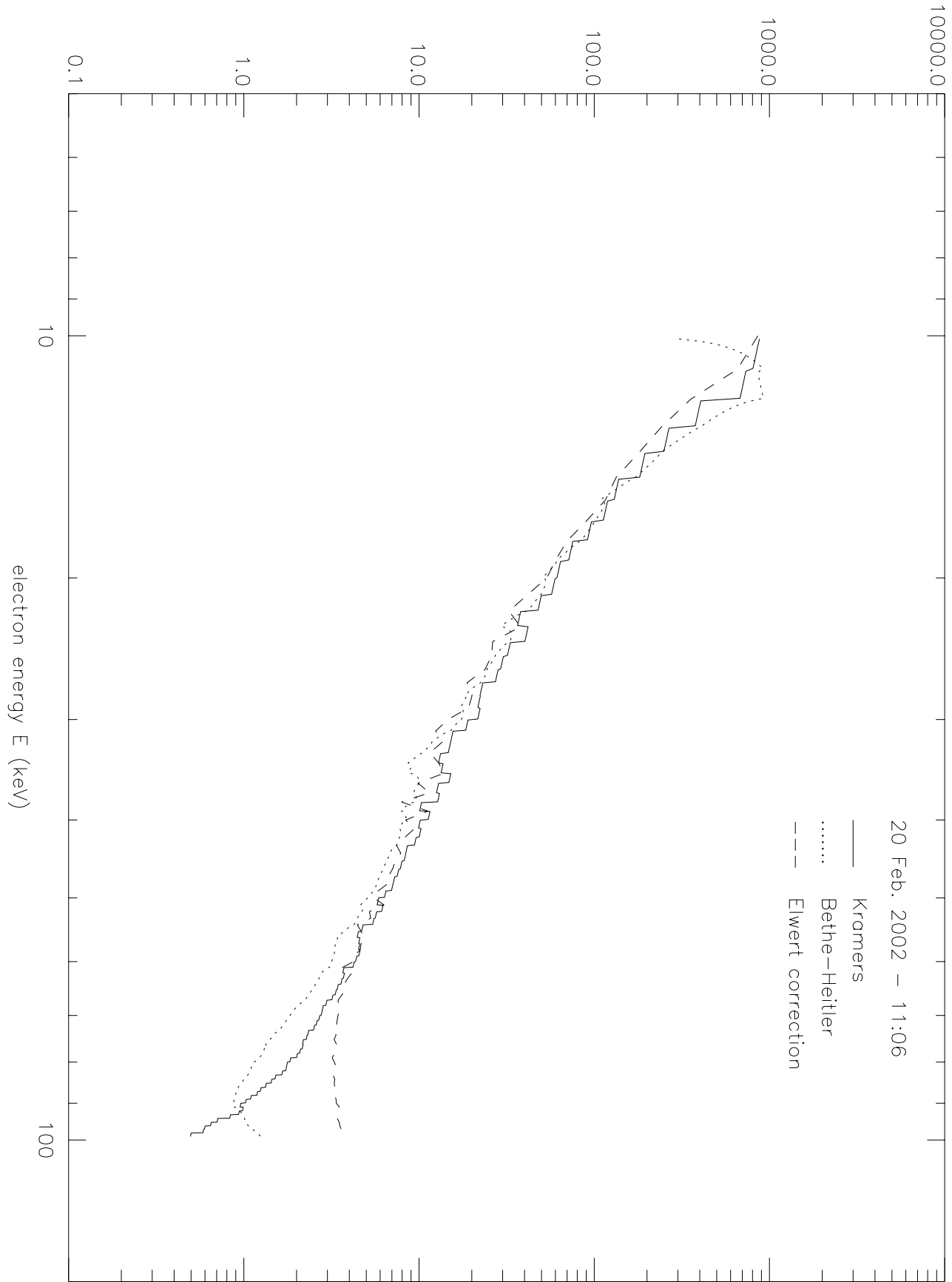


Fig. 2(a)

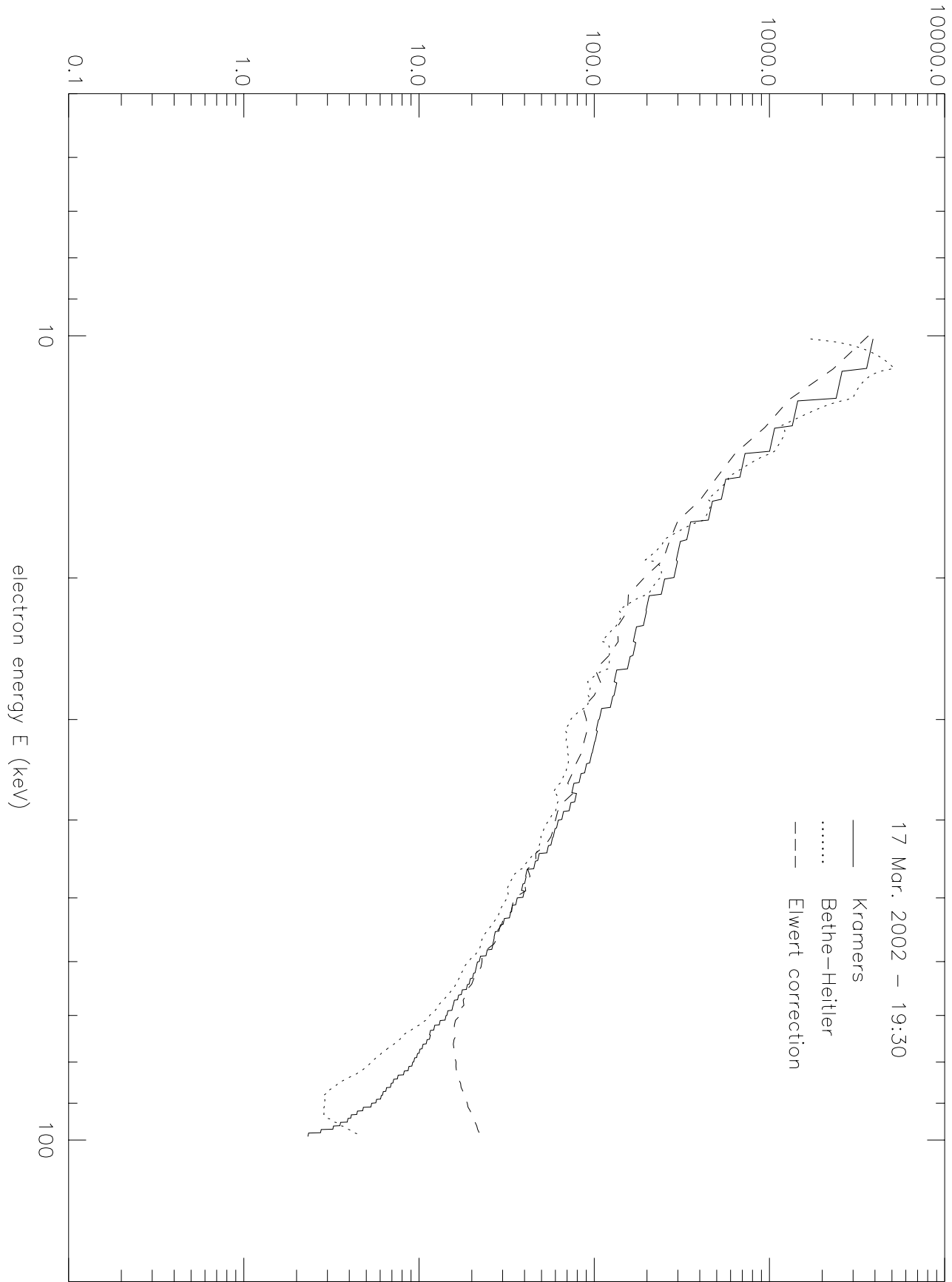


Fig. 2(b)

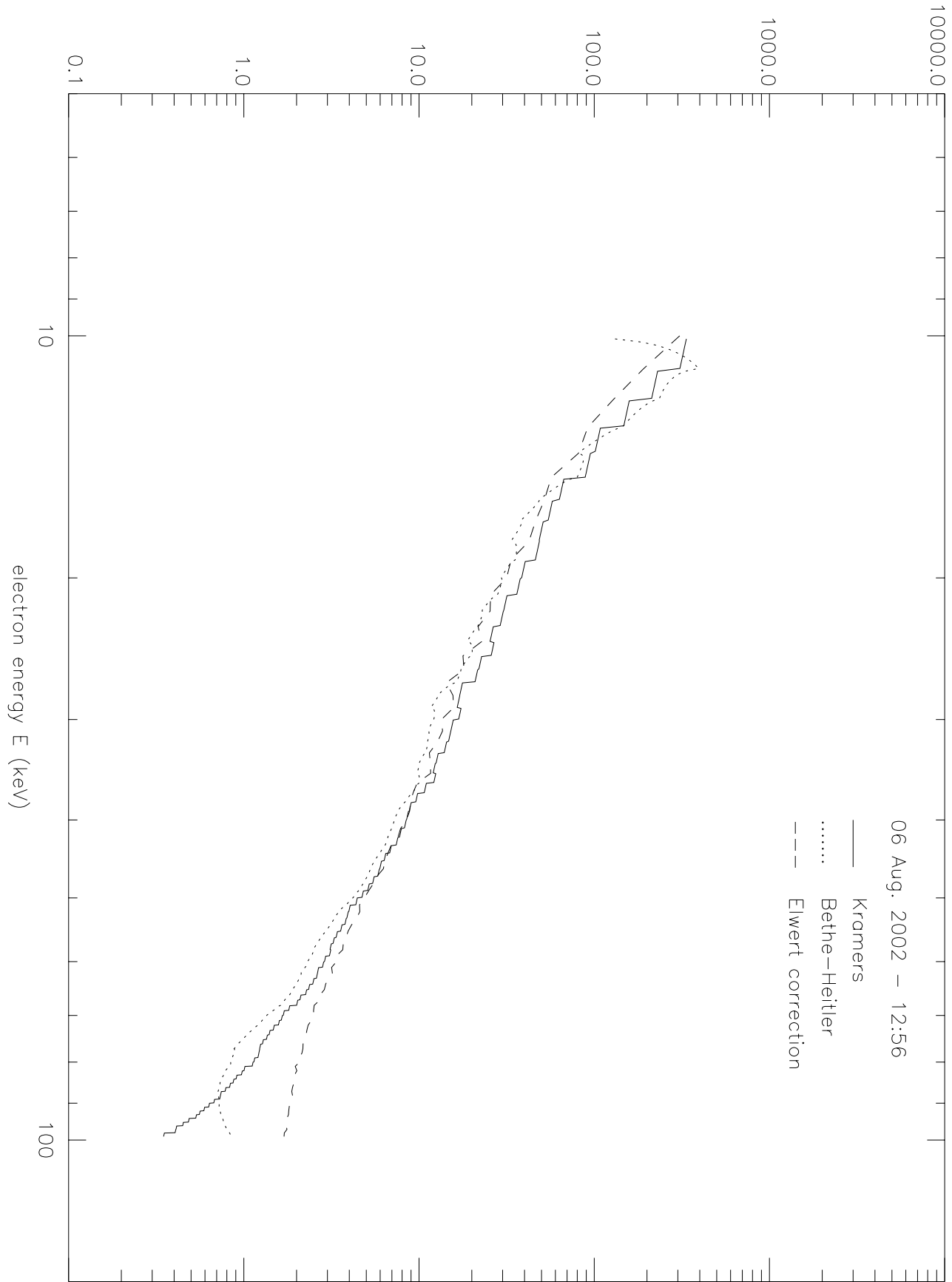


Fig. 2(c)

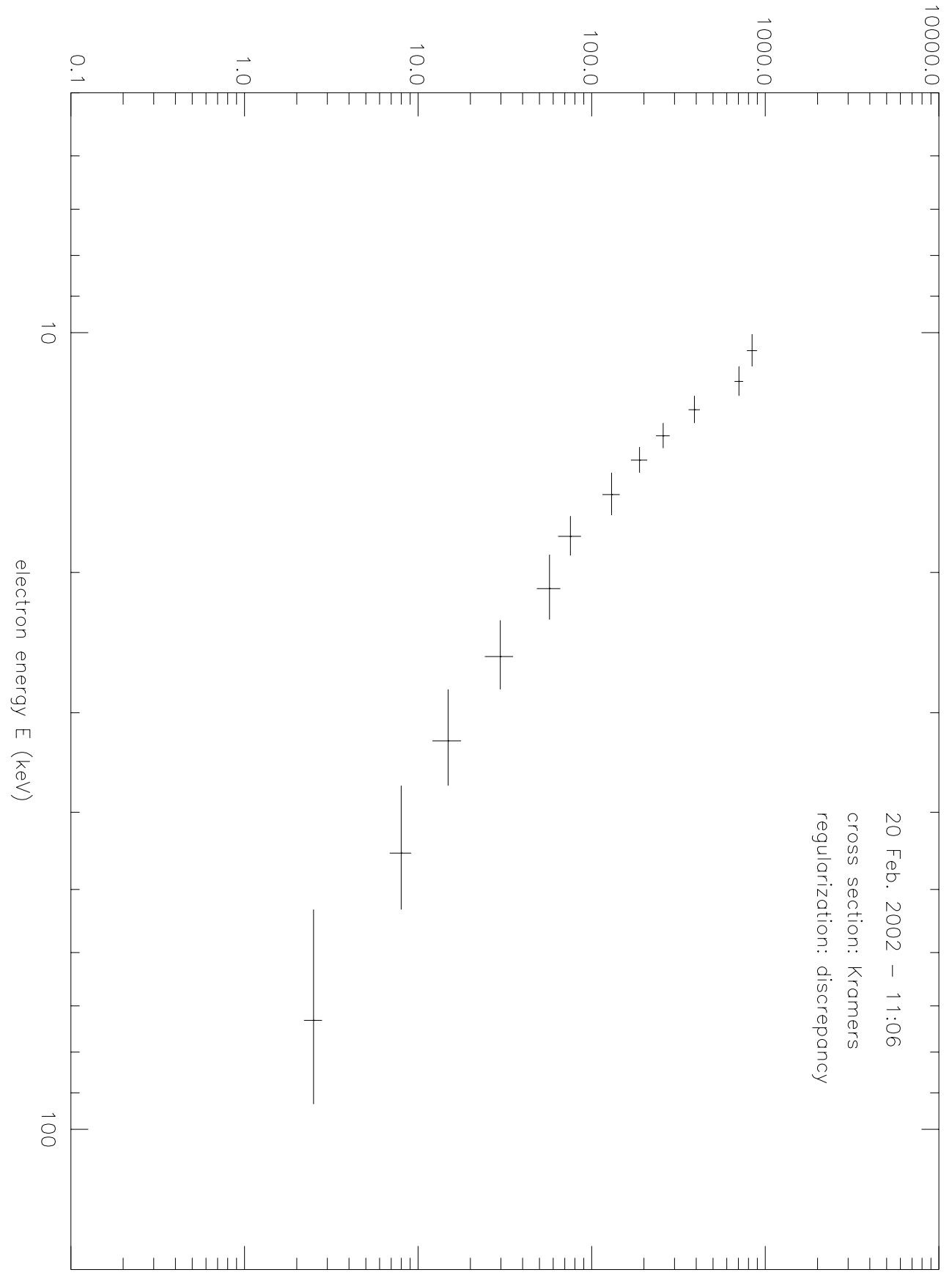


Fig. 3(a)

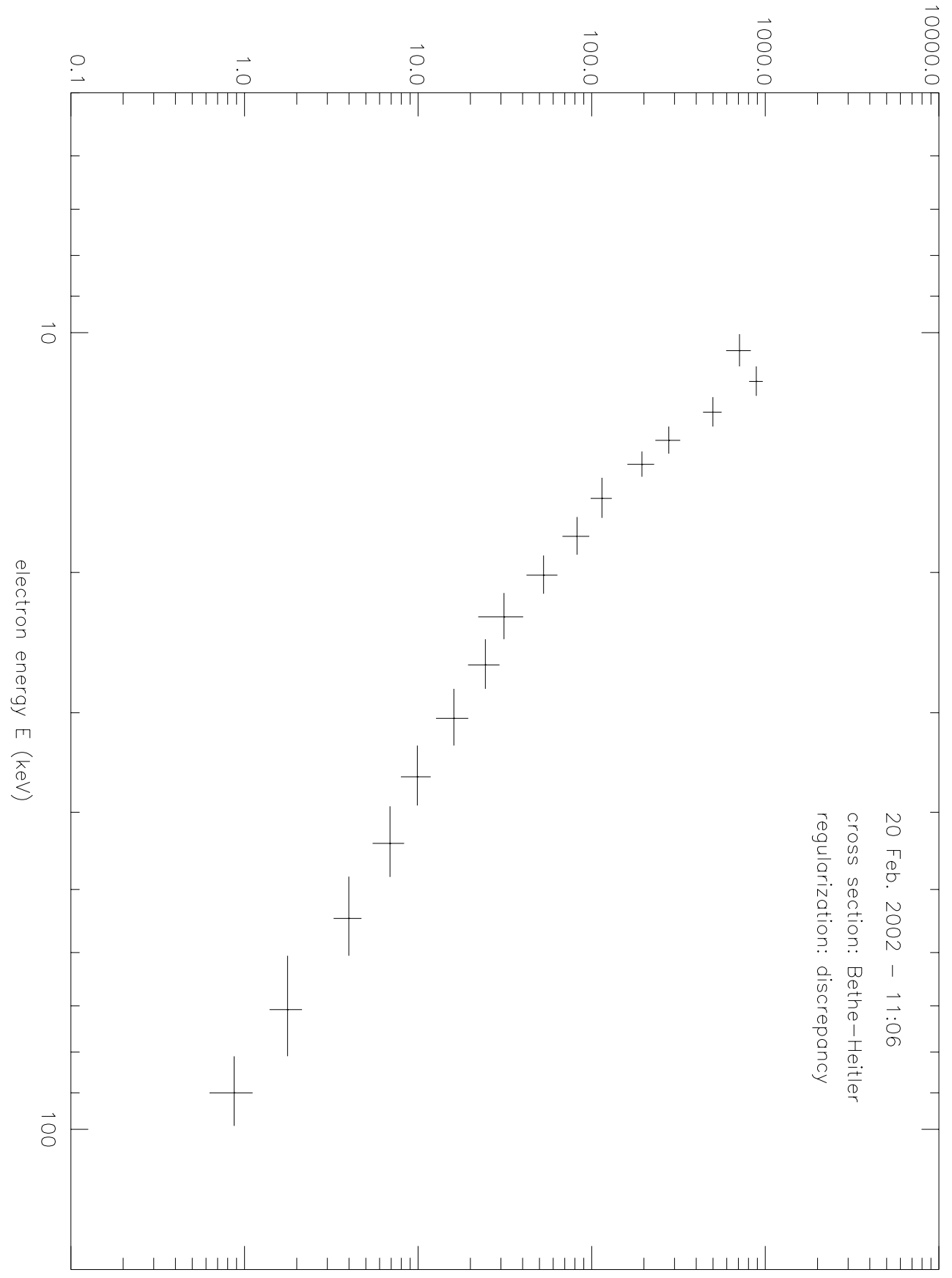


Fig. 3(b)

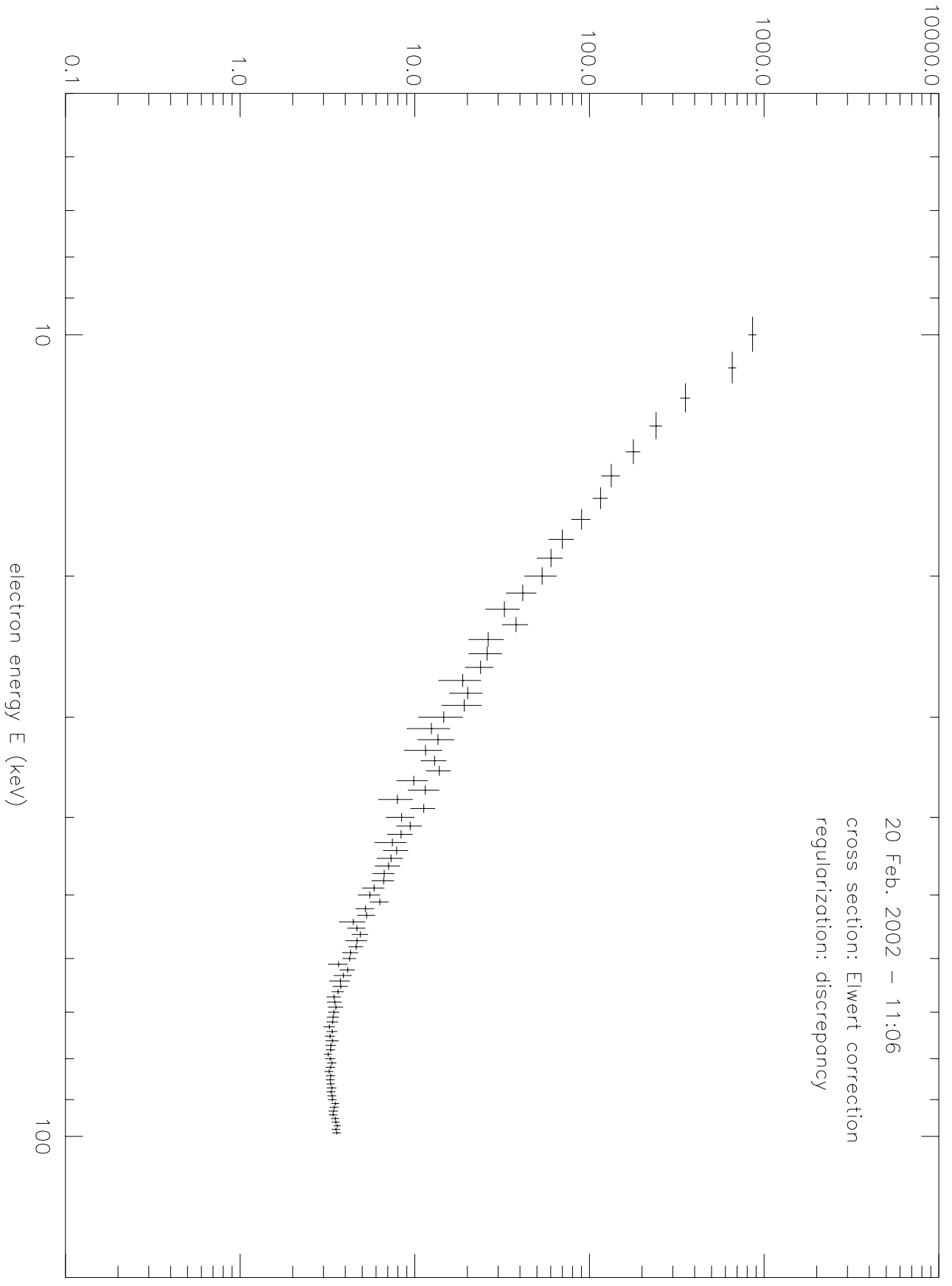


Fig. 3(c)

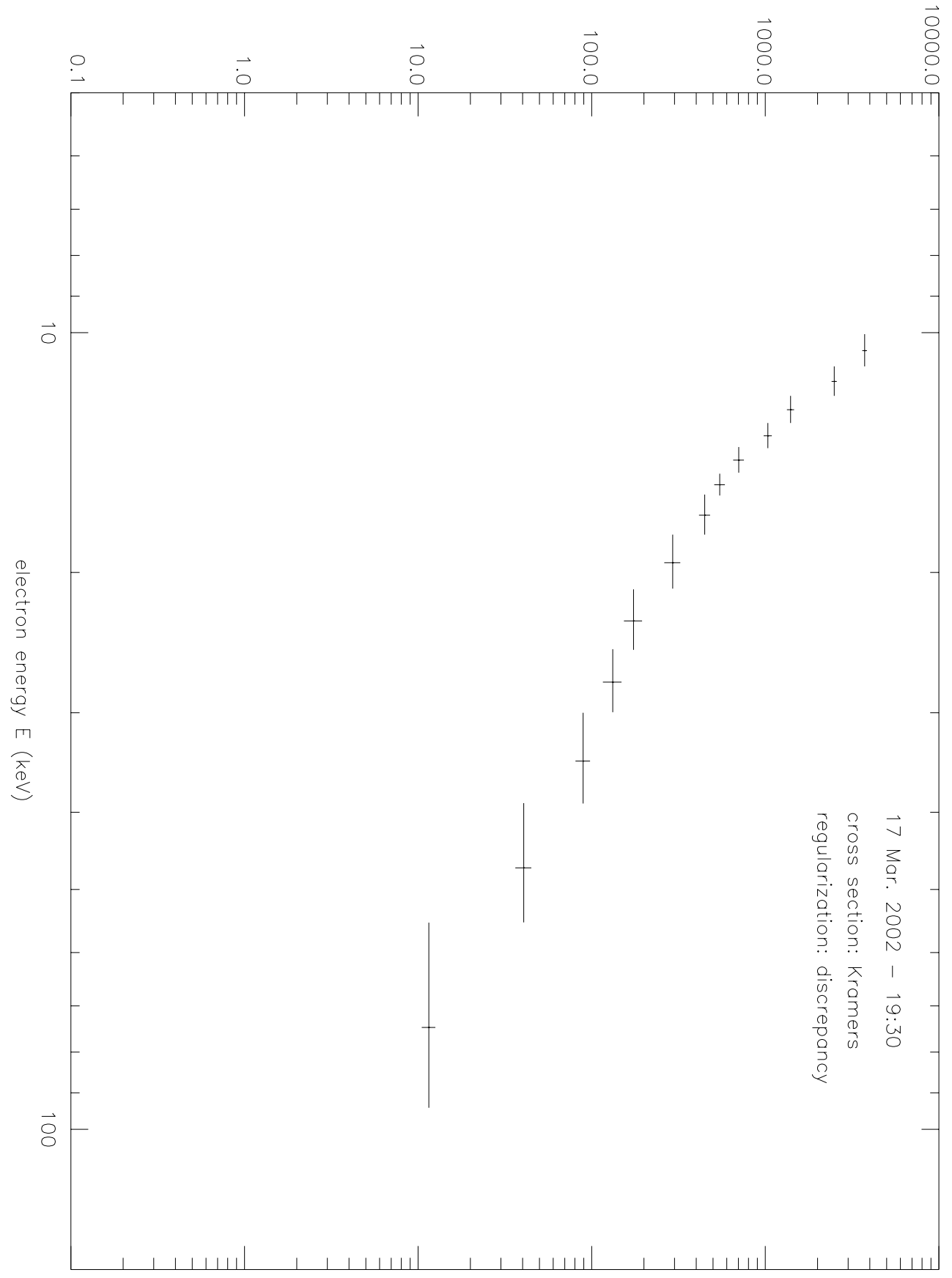


Fig. 4(a)

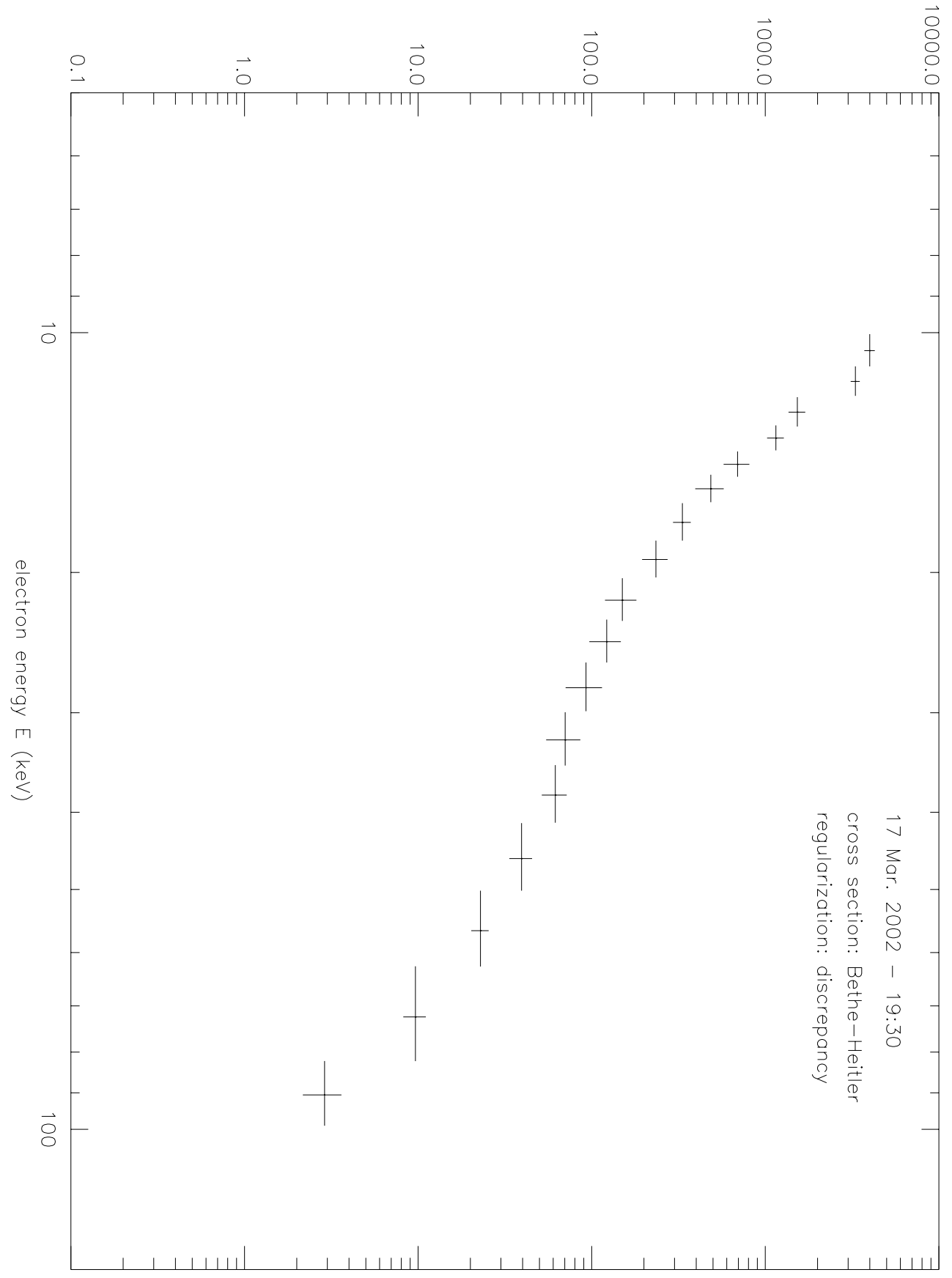


Fig. 4(b)

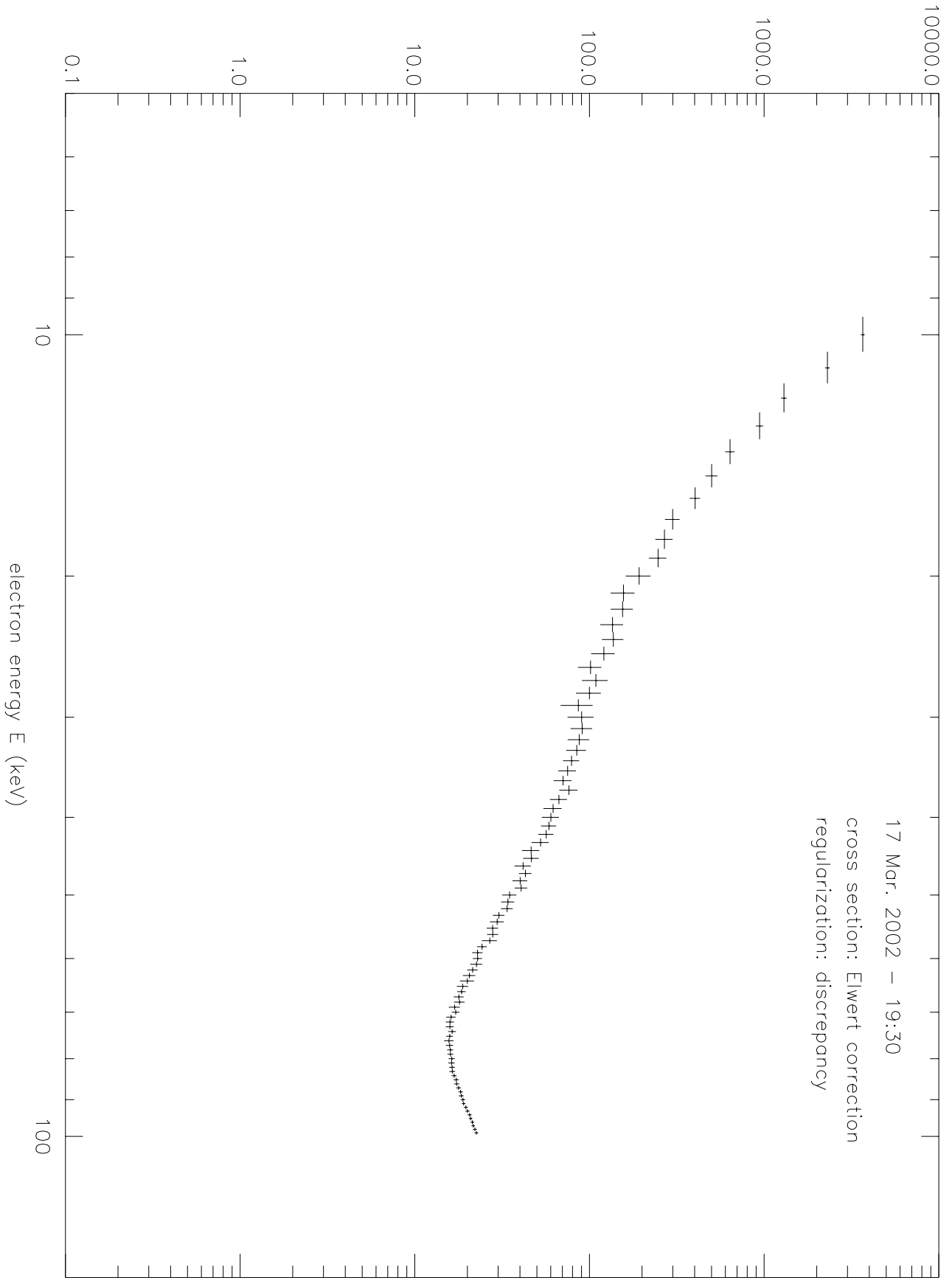


Fig. 4(c)

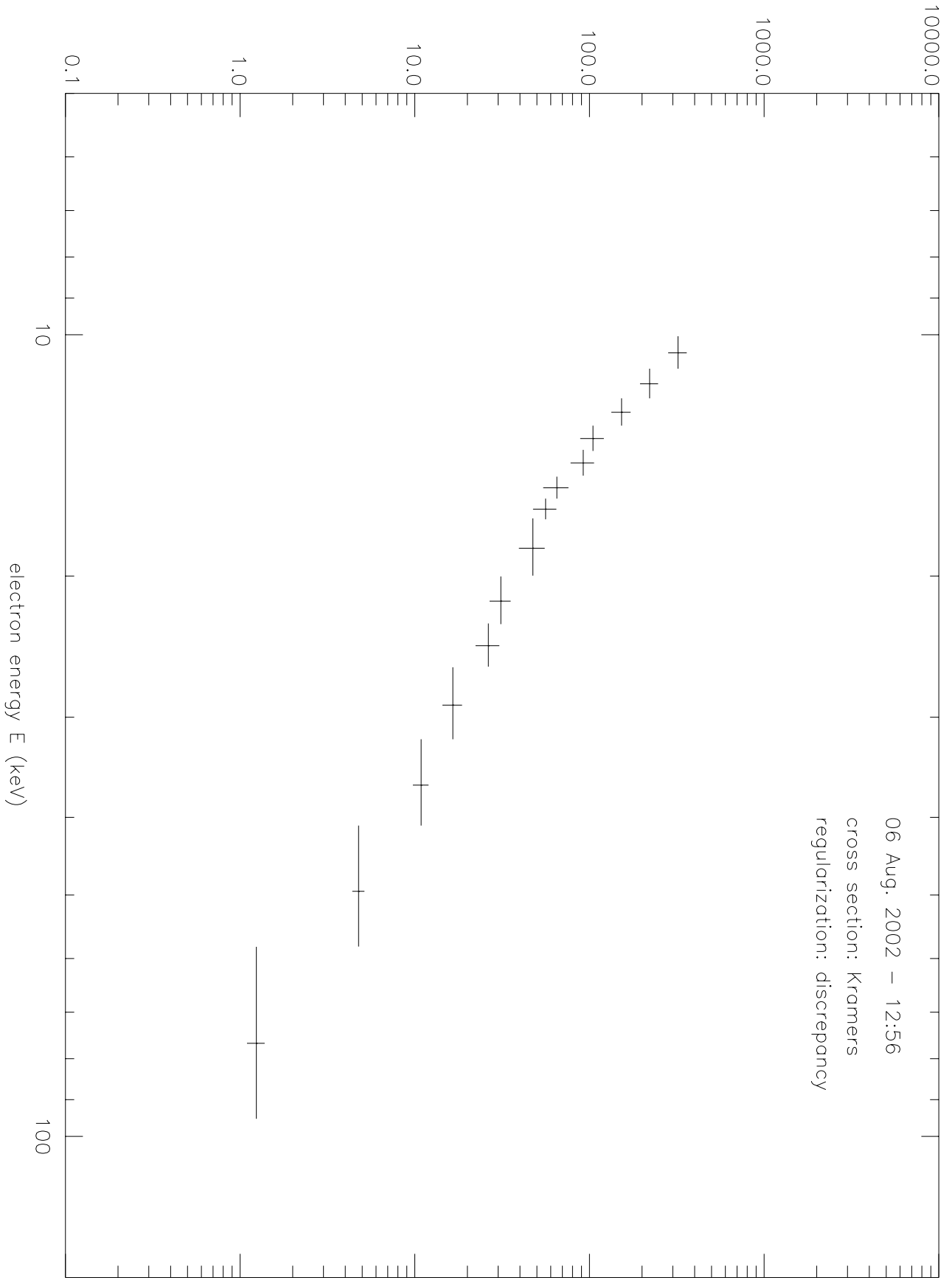


Fig. 5(a)

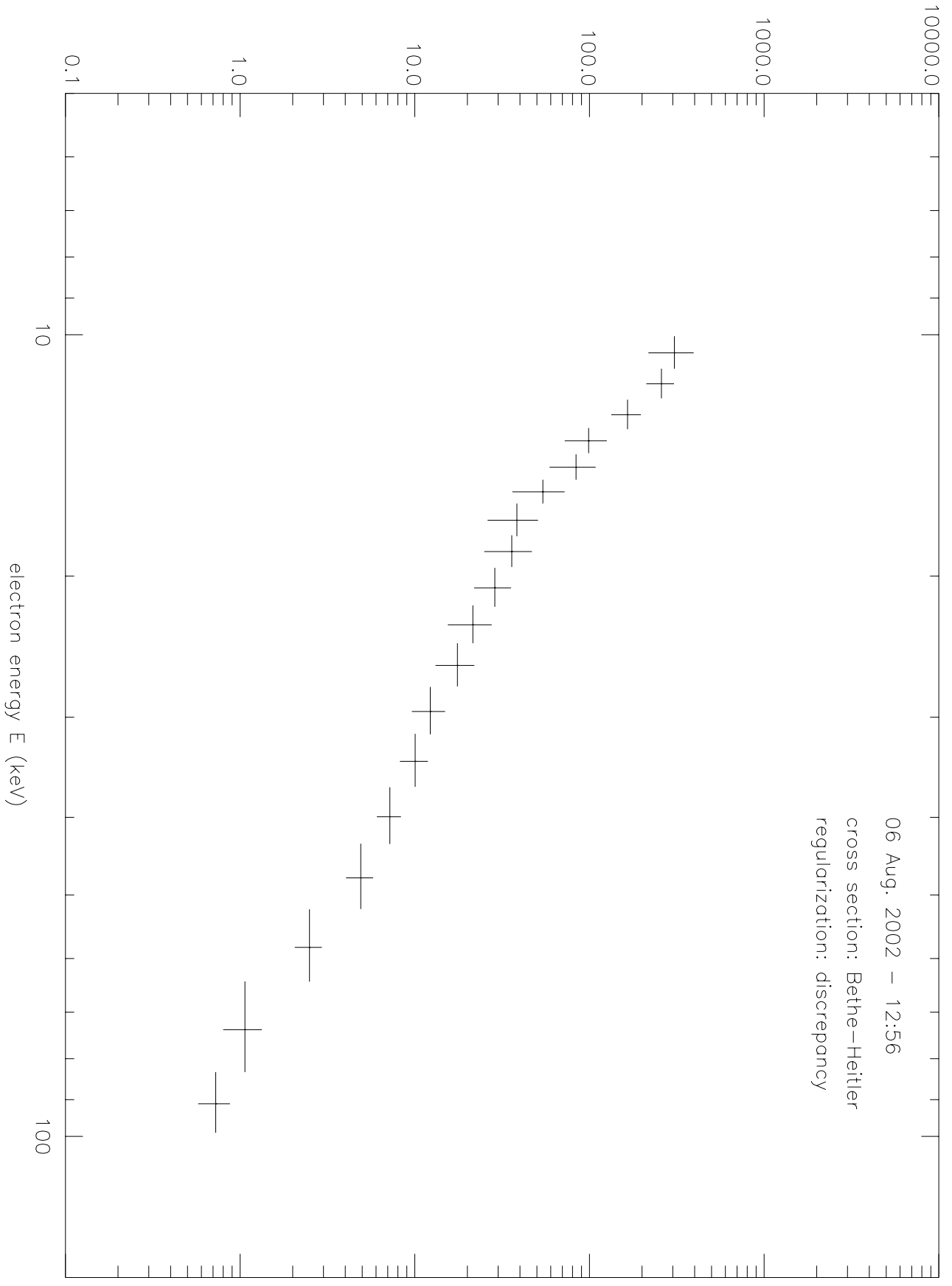


Fig. 5(b)

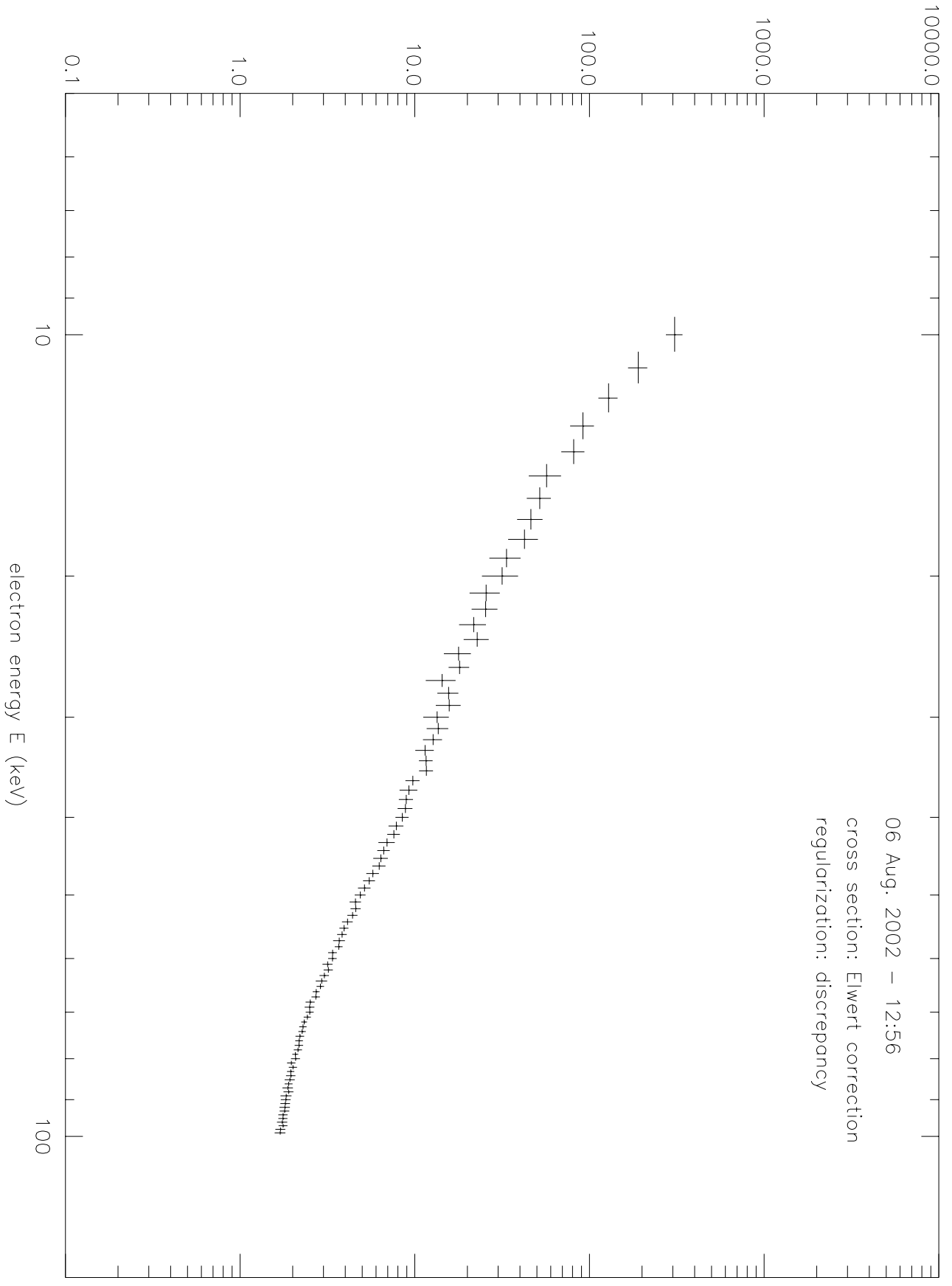


Fig. 5(c)

photon spectrum $g(\epsilon)$ ($\text{cm}^{-2} \text{s}^{-1} \text{keV}^{-1}$)

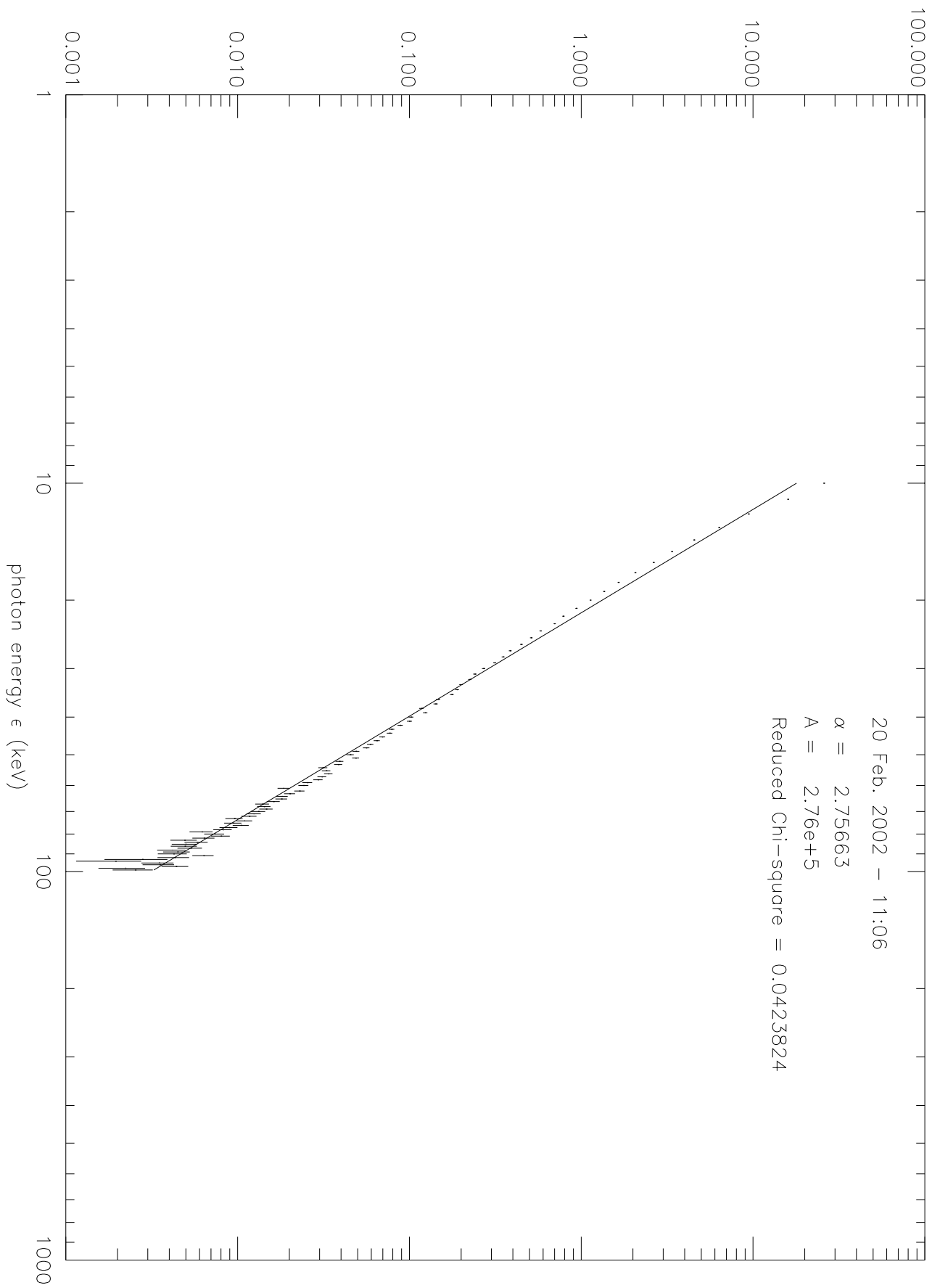


Fig. 6(a)

photon spectrum $g(\epsilon)$ ($\text{cm}^{-2} \text{s}^{-1} \text{keV}^{-1}$)

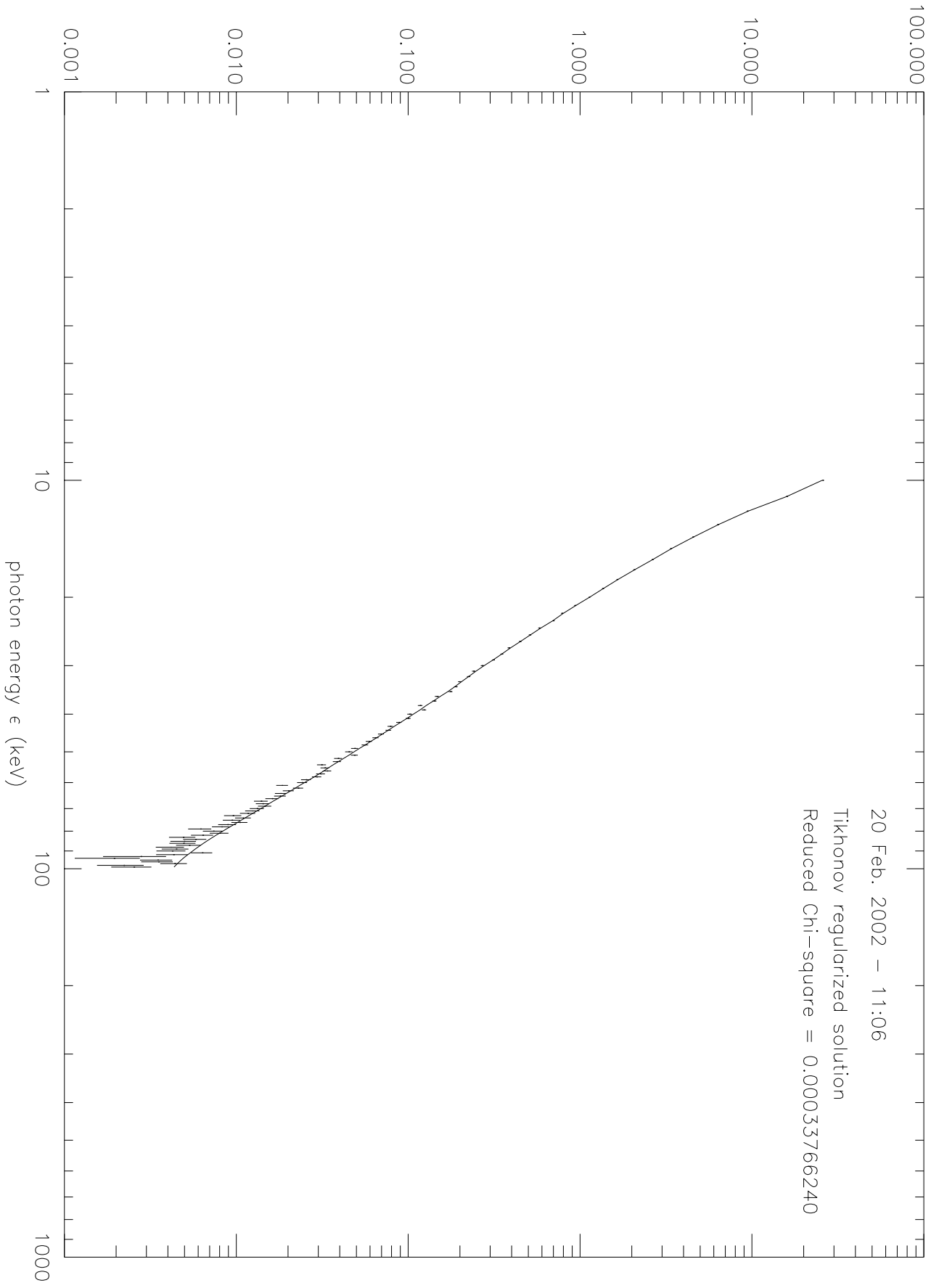


Fig. 6(b)